RSC Advances

PAPER

View Article Online
View Journal | View Issue

Cite this: *RSC Adv.*, 2014, **4**, 34649

A new type of p-type NiO/n-type ZnO nano-heterojunctions with enhanced photocatalytic activity†

Mu Xiao, Yangfan Lu,* Yaguang Li, Hui Song, Liping Zhu* and Zhizhen Ye*

Received 16th May 2014
Accepted 2nd July 2014

DOI: 10.1039/c4ra04600e

www.rsc.org/advances

A new type of NiO/ZnO nano-heterojunction was developed by the template-assisted approach. The p–n nano-heterojunctions were formed between the NiO and ZnO nanoparticles in the ultrathin shell of the NiO/ZnO hollow nanospheres. The grain size of the NiO/ZnO nano-heterojunctions is in the 10 nm scale, and the specific surface area is higher than 100 $m^2\ g^{-1}$. Moreover, the ultrathin shell makes the distribution of the NiO/ZnO nano-heterojunctions to arrange in a single-layer structure rather than a stacking arrangement. Therefore, this new type of the NiO/ZnO nano-heterojunctions could almost completely separate the electron and hole to the surface rather than being wasted in the materials. As a result, the photocatalytic activity of the p-type NiO/n-type ZnO nano-heterojunctions for the degradation of rhodamine B (RhB) was much higher than that of ZnO. In particular, the p-type NiO/n-type ZnO hollow nanospheres with different Ni/Zn molar ratios exhibited diverse catalytic activity, the mechanism of which has been discussed in detail.

Introduction

In previous decades, photocatalysis, as a "green" technique, has been widely used in the area of environmental remediation for organic pollutants.[1] By the steady and rapid growth of nanotechnology, nanostructured semiconductors have become promising candidates for photocatalysis due to their intrinsic size-dependent characteristics.[2–4] Among those nanostructured semiconductor metal oxides, zinc oxide (ZnO) nanomaterials and natural n-type semiconductors with a wide bandgap (E_g = 3.37 eV) have been recognized as excellent materials for photocatalytic processes.[5–7] However, enhancing the photocatalytic efficiency of ZnO nanocatalysts to meet practical application requirements is still a challenge because of the bottleneck of poor quantum yield caused by the rapid recombination rate of photogenerated electron–hole pairs in ZnO nanomaterials.[8] Therefore, numerous methods have been developed to increase the separation efficiency of photogenerated electron–hole pairs of ZnO nanocatalysts. Research found that ZnO-based heterojunctions, such as metal (Ag, Au, Pt, *etc.*)/ZnO and semiconductor (TiO_2, SnO_2, CdS, NiO, *etc.*)/ZnO heterojunctions, could suppress the recombination of photogenerated electron–hole pairs by the mutual transfer of photogenerated electrons or holes in the heterojunctions.[9–12]

Among these heterojunctions, the NiO/ZnO hybrids have attracted considerable interest, in particular. NiO, as a p-type semiconductor (E_g = 3.5 eV), possesses high hole concentration, high hole mobility, and low lattice mismatch with ZnO, which is beneficial for the formation of p–n heterojunction with ZnO.[12–15] Recently, nanofibers and hollow microspheres of p-type NiO/n-type ZnO with enhanced phtotcatalytic activity had been reported.[16,17] However, the precipitation conditions of the previous reports were intricate,[16,17] which means that the chemical parameters must be controlled precisely to avoid the aggregation and uneven particle size. Moreover, the inevitable stacking arrangement of each nano-heterojunction and the small specific surface area of those structures cause the separated carriers to be wasted at the boundaries between different nano-heterojunctions rather than transport to the surface.[18] Thus, such paradoxical factors make the promotion of the NiO/ZnO nano-heterojunctions photocatalytic activity to be limited. Hence, the ideal NiO/ZnO nano-heterojunctions should not only have small grain size and excellent contact crystalline quality but also have a unique structure to avoid secondary recombination, which was caused by the stacking arrangement and small surface area.

In this work, we reported a new type of NiO/ZnO nano-heterojunction, which was formed in the ultrathin shell of the NiO/ZnO hollow nanosphere. It was found that the p-type NiO/n-type ZnO nano-heterojunction has the small size in 10 nm scale. In addition, the ultrathin thickness of the shell made the nano-heterojunctions distribute in a single-layer structure rather than the stacking arrangement in previous reports. Furthermore, their surface areas were higher than 140 $m^2\ g^{-1}$.

State Key Laboratory of Silicon Materials, Department of Materials Science and Engineering, Zhejiang University, Hangzhou 310027, People's Republic of China. E-mail: yezz@zju.edu.cn; Fax: +86 571 87952625; Tel: +86 571 87952625

† Electronic supplementary information (ESI) available. See DOI: 10.1039/c4ra04600e

As a result, the recombination of the photo-generated carriers was almost completely suppressed in this new type of NiO/ZnO nano-heterojunctions. The NiO/ZnO nano-heterojunctions exhibited excellent photocatalytic activity superior to the ZnO hollow nanospheres, which could be ascribed to the ultra-high separation efficiency of photogenerated electron–hole pairs in the p–n nano-heterojunctions.

Experiment

Materials synthesis

The carbon spheres were hydrothermally synthesized using the method reported by Li.[19,20] To synthesize the p-type NiO/n-type ZnO heterojunction hollow nanospheres, 50 mg of as-prepared carbon spheres was dispersed in 100 mL deionized water by ultrasonication, followed by adding $Zn(NO_3)_2 \cdot 6H_2O$ and $Ni(NO_3)_2 \cdot 6H_2O$. The as-obtained mixture was stirred for 24 h. A rinsing process involving two cycles of centrifugation, washing and re-dispersion were performed with water and ethanol, respectively. After being dried in an oven in air at 80 °C for 6 h, the p-type NiO/n-type ZnO heterojunction hollow nanospheres were obtained by annealing the products in air at 400 °C for 12 h. The variation of the ZnO/NiO ratio in the p-type NiO/n-type ZnO heterojunction hollow nanospheres could be obtained by controlling the ratio of $Zn(NO_3)_2 \cdot 6H_2O$ and $Ni(NO_3)_2 \cdot 6H_2O$ (2 : 1, 1 : 1, 1 : 2) in the solution. The concentration of $Zn(NO_3)_2 \cdot 6H_2O$ was 0.05 M and remained constant in all experiments. In the following discussions, the p-type NiO/n-type ZnO heterojunction hollow nanospheres with original Ni/Zn molar ratios of 2 : 1, 1 : 1 and 1 : 2 were denoted as A, B and C, respectively.

Characterization

Crystallographic phases of all the products were examined by XRD (X'Pert PRO) using Cu Ka line (1.540598 nm for Cu Ka1 and 1.544426 nm for Cu Ka2) at the excitation voltage of 40 kV and tube current of 40 mA. UV-vis absorption experiments were carried out on UV-vis spectroscopy (Shimadzu UV3600). Raman spectroscopy was detected with a Jobin Yvon HR800 micro-Raman spectrometer using a 325 nm line from a He–Cd laser. Morphologies of the samples were carried out by field emission scanning electron microscopy (FESEM, Hitachi S-4800). Survey TEMs were conducted using a JEOL JEM 1230 transmission electron microscope operated at 80 kV and a Philips CM 200 microscope operated at 160 kV. High-resolution TEM (HRTEM) and energy-dispersive X-ray spectroscopy (EDX) were performed on a FEI TECNAI G 2 F20 transmission electron microscope operated at 200 kV. Samples for TEM analyses were prepared by dropping a dilute solution of hollow nanospheres onto ultra-thin carbon-coated copper grids. Nitrogen adsorption–desorption measurements were performed at 77 K using an ASAP 2010 analyzer utilizing the BET model for the calculation of surface areas. Room-temperature photoluminescence (PL) measurement was carried out with excitation by a 325 nm line of a He–Cd laser to evaluate the optical property of p-type NiO/n-type ZnO heterojunction hollow nanospheres.

Photocatalytic test

The photoreactor was designed with an internal light source surrounded by a quartz jacket where the suspension included the hollow nanospheres catalyst (0.05 g), and an aqueous RB (100 mL, 10 mg L^{-1}) completely surrounded the light source. The suspension was stirred in darkness for 30 min to obtain a good dispersion and establish adsorption–desorption equilibrium between the organic molecules and the catalyst surfaces. The temperature of the suspension was maintained at 30 ± 2 °C by circulating water through an external cooling coil, and the system was open to the air. The suspension was exposed to the irradiation of a 300 W ultraviolet (UV) lamps (WFH-203, maximum emission at 365 nm and an average light intensity of 0.7 mW cm^{-2}) at room temperature. After that, a 3 mL sample of the suspension was taken out at regular intervals and centrifuged to completely remove the catalyst. The measurement of RhB degradation was then carried out on a UV-vis spectroscopy (Shimadzu UV3600). Similar experiments were performed by using 50 mg pure ZnO hollow nanospheres as a photocatalyst under the same conditions for comparison.

Results and discussion

The X-ray diffraction (XRD) analysis was carried out for the hollow nanospheres to identify their crystal phases. As observed in Fig. 1, three sets of diffraction peaks existed for A, B and C hollow nanospheres, which were correspondingly ascribed to the cubic structure NiO and hexagonal structure ZnO. No characteristic peaks for impurity were observed, indicating that the composition of the above hollow nanospheres was NiO and ZnO. It is noteworthy that the diffraction peaks of NiO and ZnO in the A, B and C were still sharp and intense, implying the high crystallinity of the NiO/ZnO heterojunction hollow nanospheres. Raman spectra further confirmed the composition of all the samples in Fig. S1.†

Fig. 2a–c showed the scanning electron microscopy (SEM) images of the A, B and C respectively. It could be seen that

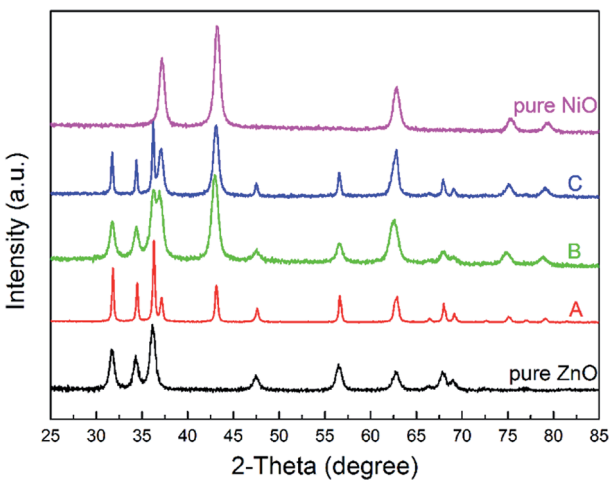

Fig. 1 XRD patterns of the p-type NiO/n-type ZnO nano-heterojunction hollow nanospheres.

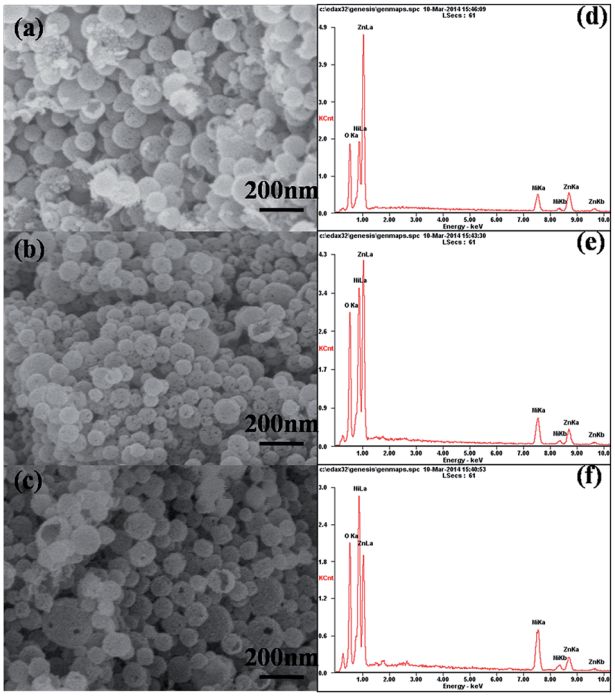

Fig. 2 (a–c) SEM images of p-type NiO/n-type ZnO nano-heterojunction hollow nanospheres for sample A, B and C and (d–f) the corresponding EDX spectrum for A, B and C.

perfect hollow nanospheres for the A, B and C were obtained. The average diameter of the hollow nanospheres could reach to 240 nm. Moreover, Fig. 2d–f showed the energy-dispersive X-ray (EDX) spectra from Fig. 2a–c, respectively. It was further confirmed that the A, B and C hollow nanospheres were composed of Ni, Zn, and O. In addition, as shown in Table 1, EDX analysis indicated that the molar ratios of Ni to Zn were about 0.43 for sample of A, 0.92 for B and 1.62 for C, which were close to the original value.

In order to study the morphology and microstructure of the NiO/ZnO hollow nanospheres in detail, high-resolution transmission electron microscopy (HRTEM) observations were carried out. Fig. 3 showed the representative TEM images of the p-type NiO/n-type ZnO heterojunction hollow nanospheres. The low-magnification TEM image of the p-type NiO/n-type ZnO heterojunction hollow nanospheres was shown in Fig. 3a. It could be seen clearly that the perfect hollow nanospheres were composed of many nanoparticles attached to each other. Meanwhile, Fig. 3b–d displayed high-resolution images of the sample A, B and C, which reveals the simultaneous presence of the crystalline NiO and ZnO crystal lattices in the hollow nanospheres. The interplanar distances of 0.209 nm and 0.208

Table 1 The contents of Zn^{2+} and Ni^{2+} for the samples of A, B and C

Sample	A	B	C
Zn content (%)	43.88	26.24	24.01
Ni content (%)	18.65	22.19	35.72

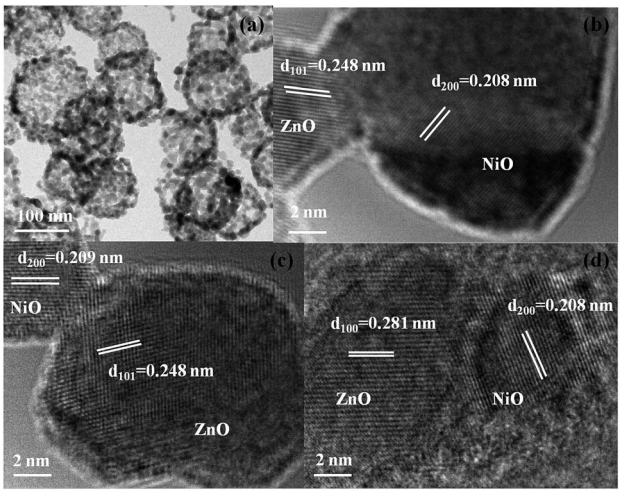

Fig. 3 (a) TEM image and (b–d) HRTEM of p-type NiO/n-type ZnO nano-heterojunction region in A, B and C.

nm were close to the *d* spacings of the (2 0 0) planes of the cubic-structured NiO. The interplanar distances of 0.248 nm and 0.281 nm agreed well with the lattice spacing of the (101) and (100) planes of the hexagonally structured ZnO, respectively. Furthermore, a distinguished interface between the NiO and ZnO nanoparticles and the continuity of lattice fringes belonging to NiO and ZnO could be observed in Fig. 3b–d, suggesting that the p–n heterojunction had been formed between the NiO and ZnO nanoparticles in the p-type NiO/n-type ZnO hollow nanospheres. Moreover, as shown in Fig. 3b–d, the grain sizes of the sample A, B and C were about 17 nm, 12 nm and 6 nm, respectively. It indicated that the grain size decreased as the Ni content increased. The textural feature of the samples A, B and C was further measured by nitrogen sorption measurement at 77 K. Fig. 4 showed the Brunauer–Emmett–Teller (BET) surface area of sample C could be as high as 148 $m^2\ g^{-1}$. This could be explained that the hollow nanospheres are composed of nanoparticles, thus a high surface area

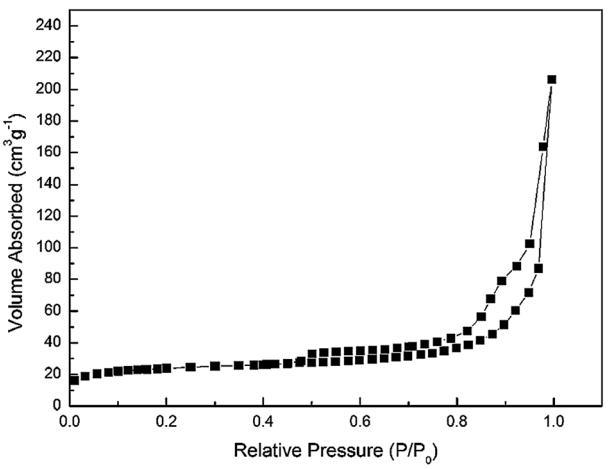

Fig. 4 N_2 adsorption–desorption isotherm of sample C.

could be obtained. The BET surface areas of the other composite hollow nanospheres were about 127 and 132 $m^2 g^{-1}$ for samples A and B, respectively (Fig. S2†). Thus, the smaller the crystal size, the larger the BET surface area of the sample.

Fig. 5 showed the UV-vis absorption spectroscopy of the ZnO, NiO, A, B and C hollow nanospheres. The strong absorption peaks of NiO and ZnO were observed. Moreover, all of the characteristic absorption peaks of NiO and ZnO existed in the UV-vis absorption spectroscopy of the samples A, B and C. It confirmed that the NiO/ZnO heterojunction hollow nanospheres were composite materials that consisted of NiO and ZnO.

On the basis of the aforementioned experimental results and the theory analysis, a proposed energy band structure diagram of the p-type NiO/n-type ZnO heterojunction was elucidated schematically in Fig. 6. When the p-type NiO and n-type ZnO formed the p–n nano-heterojunction, an inner electrical field was built in the interface between NiO and ZnO because of the electron and hole transfers. Furthermore, due to the small grain size, no neutral regions existed in this nano-heterojunction system. Thus, when the valence electrons were excited by UV light, it could be determined that the photo-generated electrons and holes were transferred to the CB of ZnO and the VB of NiO, respectively. That is, the photo-generated electrons and holes were completely separated to the surfaces of NiO and ZnO nanoparticles, respectively, by the inner electrical field.

To verify the separated efficiency, Fig. 7 displayed the PL spectra of pure ZnO, A, B and C hollow nanospheres. For pure ZnO, the near-band edge UV emission located at 380 nm can be ascribed to the recombination of free excitons. The broad visible emissions ranging from 550 to 750 nm corresponded to the deep level of the trap-state emission of ZnO. Compared with pure ZnO hollow nanospheres, the NiO/ZnO hollow nanospheres exhibit negligible emission intensity. This phenomenon indicated that the recombination of the photogenerated electron–hole pairs was significantly suppressed in the p-type NiO/n-type ZnO nano-heterojunctions. The prolonged lifetime of photogenerated electron–hole pairs through the effective charge separation would facilitate the interfacial charge transfer between NiO and ZnO, leading to the enhanced photocatalytic activity of the p-type NiO/n-type ZnO nano-heterojunctions hollow nanospheres.

To further confirm the effective charge separation of the nano-heterojunctions, the activities of p-type NiO/n-type ZnO nano-heterojunctions hollow nanospheres for the degradation of the rhodamine B (RhB) were investigated. In Fig. 8a, an obvious degradation of RhB was observed under UV light in the presence of the nano-heterojunctions (C hollow nanospheres). The comparative experiments were carried out in this test: (1) blank, with UV light irradiation and in the absence of the photocatalysts; and (2) dark, in the presence of the photocatalysts under no light irradiation. As shown in Fig. 8b, these results revealed that there was no appreciable degradation of RhB after 200 min either in the absence of photocatalysts or in the absence of UV light irradiation. Furthermore, in comparative experiments, the NiO and ZnO hollow nanospheres were

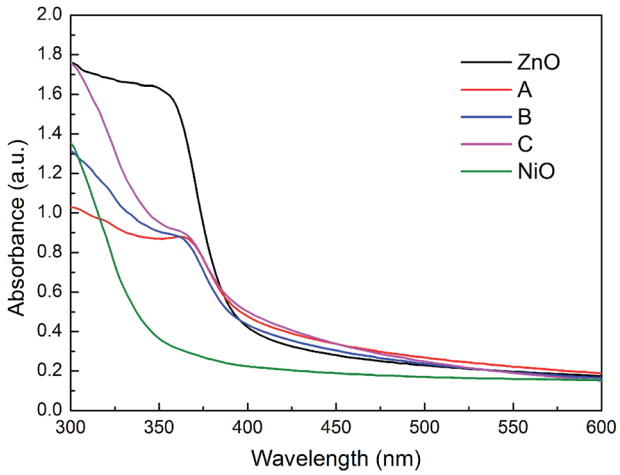

Fig. 5 UV-vis adsorption spectra of ZnO, NiO, A, B and C samples.

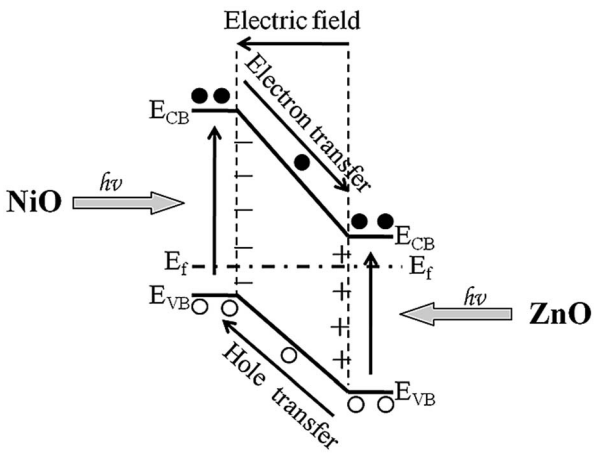

Fig. 6 Schematic diagram showing the energy band structure and electron–hole pair separation in the p-type NiO/n-type ZnO.

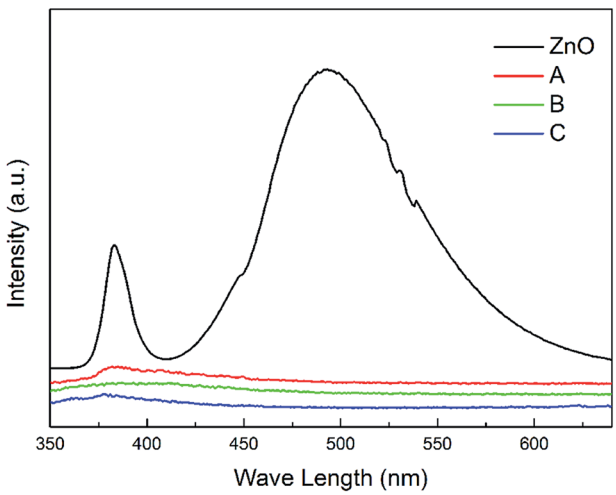

Fig. 7 PL emission spectra of ZnO, A, B and C.

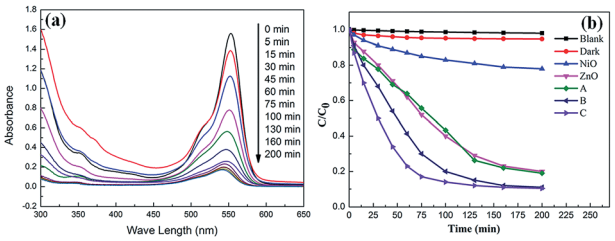

Fig. 8 (a) UV-vis spectra of the aqueous solutions of RhB after UV irradiation for different time periods in the presence of C. (b) Photodegradation of RhB of ZnO, NiO, A, B and C samples.

used as a photocatalytic reference to understand the photocatalytic activity of the p-type NiO/n-type ZnO nano-heterojunction. As shown in Fig. 8b, the degradation efficiency of RhB was about 15%, 48%, 44.3%, 70%, and 83% for the NiO, ZnO, A, B, and C hollow nanospheres after 75 min, respectively. Notably, the decolourization efficiency of RhB over the C hollow nanospheres was over 80%, which was much higher than the corresponding degradation time of A, B ZnO and NiO hollow nanospheres, suggesting that the C hollow nanospheres exhibited the highest photocatalytic activity among those hollow nanospheres. According to the TEM analysis, the grain size of C was smaller than that of the other samples. In combination with the theoretical analysis, the smaller the grain size, the better separated efficiency of the p–n nano-heterojunctions. Thus, the excellent behavior of sample C may be attributed to the influence of the small grain size.

Conclusion

In summary, with the assistance of the carbon spheres template, p-type NiO/n-type ZnO nano-heterojunctions with different molar ratios of Ni to Zn were successfully fabricated. The new type of nano-heterojunction has the small size in 10 nm scale single, higher surface area than 140 $m^2 g^{-1}$ and single-layer distribution structure. The PL emission test confirmed that the photogenerated electron–hole pairs were almost completely separated in this nano-heterojunctions. And the NiO/ZnO nano-heterojunctions possessed higher photocatalytic activity than the pure NiO and ZnO hollow nanospheres for the degradation of RhB dye under UV light irradiation.

Acknowledgements

This work was supported by National Natural Science Foundation of China under Grant no. 51172204, 51202217, 91333203, Doctoral Fund of Ministry of Education of China under Grant no. 20120101120116, Program for Innovative Research Team in University of Ministry of Education of China under Grant No. IRT13037, and Science Technology Department Project of Zhejiang Province under Grant no. 2010R50020.

Notes and references

1 R. Asahi, T. Morikawa, T. Ohwaki, K. Aoki and Y. Taga, *Science*, 2001, **293**, 269–271.
2 M. R. Hoffmann, S. T. Martin, W. Choi and D. W. Bahnemann, *Chem. Rev.*, 1995, **95**, 69–96.
3 A. Testino, I. R. Bellobono, V. Buscaglia, C. Canevali, M. D'Arienzo, S. Polizzi, R. Scotti and F. Morazzoni, *J. Am. Chem. Soc.*, 2007, **129**, 3564–3575.
4 K.-I. Katsumata, C. E. J. Cordonier, T. Shichi and A. Fujishima, *J. Am. Chem. Soc.*, 2009, **131**, 3856–3857.
5 E. S. Jang, J. H. Won, S. J. Hwang and J. H. Choy, *Adv. Mater.*, 2006, **18**, 3309–3312.
6 A. McLaren, T. Valdes-Solis, G. Li and S. C. Tsang, *J. Am. Chem. Soc.*, 2009, **131**, 12540–12541.
7 L. Xu, Y.-L. Hu, C. Pelligra, C.-H. Chen, L. Jin, H. Huang, S. Sithambaram, M. Aindow, R. Joesten and S. L. Suib, *Chem. Mater.*, 2009, **21**, 2875–2885.
8 L. Zheng, Y. Zheng, C. Chen, Y. Zhan, X. Lin, Q. Zheng, K. Wei and J. Zhu, *Inorg. Chem.*, 2009, **48**, 1819–1825.
9 Q. Wang, B. Geng and S. Wang, *Environ. Sci. Technol.*, 2009, **43**, 8968–8973.
10 Y. Zheng, L. Zheng, Y. Zhan, X. Lin, Q. Zheng and K. Wei, *Inorg. Chem.*, 2007, **46**, 6980–6986.
11 X. Wang, G. Liu, Z.-G. Chen, F. Li, L. Wang, G. Q. Lu and H.-M. Cheng, *Chem. Commun.*, 2009, 3452–3454.
12 F. Tian and Y. Liu, *Scr. Mater.*, 2013, **69**, 417–419.
13 J.-Y. Wang, C.-Y. Lee, Y.-T. Chen, C.-T. Chen, Y.-L. Chen, C.-F. Lin and Y.-F. Chen, *Appl. Phys. Lett.*, 2009, **95**, 131117(1)–131117(3).
14 H. Ohta, M. Hirano, K. Nakahara, H. Maruta, T. Tanabe, M. Kamiya, T. Kamiya and H. Hosono, *Appl. Phys. Lett.*, 2003, **83**, 1029–1031.
15 L. Qiao, X. Wang, X. Sun, X. Li, Y. Zheng and D. He, *Nanoscale*, 2013, **5**, 3037–3042.
16 Z. Zhang, C. Shao, X. Li, C. Wang, M. Zhang and Y. Liu, *ACS Appl. Mater. Interfaces*, 2010, **2**, 2915–2923.
17 Q. Xie, H. Guo, X. Zhang, A. Lu, D. Zeng, Y. Chen and D.-L. Peng, *RSC Adv.*, 2013, **3**, 24430–24439.
18 E. H. Sargent, *Nat. Photonics*, 2012, **6**, 133–135.
19 X. Sun and Y. Li, *Angew. Chem., Int. Ed.*, 2004, **43**, 597–601.
20 X. Sun, J. Liu and Y. Li, *Chem.–Eur. J.*, 2006, **12**, 2039–2047.